SCIENCE CHINA PRESS

SCIENCE CHINA Life Sciences
life.scichina.com link.springer.com
https://doi.org/10.1007/s11427-025-2954-3

RESEARCH PAPER

Mitochondrial stress orchestrates chromatin remodeling and longevity via phosphoregulation of the NuRD component LIN-40

Jun Zhou[1†], Di Zhu[1†], Yibing Wang[1,2], Zilun Wang[1], Ning Zhang[1], Xiahe Huang[1], Yiqian Zhang[1], Yingchun Wang[1], Xueying Wu[1*] & Ye Tian[1,2*]

[1]Institute of Genetics and Developmental Biology, Chinese Academy of Sciences, Beijing 100101, China
[2]University of Chinese Academy of Sciences, Beijing 100093, China

†Contributed equally to this work
*Corresponding authors (Xueying Wu, email: xueyingwu@genetics.ac.cn; Ye Tian, email: ytian@genetics.ac.cn)

Received 30 April 2025; Accepted 6 May 2025; Published online 13 August 2025

Mitochondrial dysfunction is a hallmark of aging that elicits adaptive nuclear responses, yet how chromatin remodeling is coordinated under stress remains unclear. Here, we uncover a phosphorylation-dependent mechanism by which mitochondrial stress regulates the activity of the NuRD (nucleosome remodeling and deacetylase) complex via LIN-40, the *Caenorhabditis elegans* homolog of mammalian MTA proteins. Mitochondrial stress triggers dephosphorylation of LIN-40, enhancing its interaction with the transcription factor DVE-1 to activate the mitochondrial unfolded protein response (UPR^{mt}) and chromatin remodeling. Phosphorylation of LIN-40 is mediated by p38 MAPK/PMK-3 and reversed by PP1c/GSP-2. Furthermore, the LIN-40(T654D) variant abolishes mitochondrial stress-induced lifespan extension. These findings establish a direct link between mitochondrial stress signaling and chromatin remodeling via NuRD, revealing an evolutionarily conserved strategy to coordinate cellular resilience and organismal longevity.

mitochondrial stress | NuRD | LIN-40/MTA | UPR^{mt} | longevity | *C. elegans*

INTRODUCTION

Organisms regulate key life processes through mechanisms that sense their nutritional state and environment and respond to internal and external stimuli. Several of these processes can extend lifespan (Green et al., 2022; Roh et al., 2016; Sujkowski et al., 2022; Templeman and Murphy, 2018). Mitochondria, the cellular energy hubs, are crucial for sensing various stress conditions and generating signal molecules that fine-tune cellular homeostasis (Shen et al., 2022; Tan and Finkel, 2020). Mitochondrial metabolites, DNA, proteins, and lipids could act as key sensors that regulate adaptive cellular responses (Mottis et al., 2019; Picard and Shirihai, 2022). This mitochondrial stress response pathway plays a central role in metabolism, immunity, stress response, and aging (Cai et al., 2022; Lima et al., 2022; López-Otín et al., 2013; López-Otín et al., 2023).

Studies in *C. elegans*, *Drosophila*, and mice have shown that mild mitochondrial stress can extend lifespan (Chen et al., 2024; Copeland et al., 2009; Dillin et al., 2002; Lee et al., 2003; Liu et al., 2005; Rea et al., 2007). The mitochondrial unfolded protein response (UPR^{mt}), a conserved transcriptional response activated in response to disrupted mitochondrial proteostasis, plays a crucial role in this longevity pathway by mediating mitochondrial-to-nuclear communication (Shpilka and Haynes, 2018; Zhu et al., 2022). In *C. elegans*, disruption of the electron transport chain (ETC) alters mitochondrial membrane potential, leading to UPR^{mt} activation via the transcription factor ATFS-1, which accumulates in the nucleus when blocked from entering the mitochondria (Haynes et al., 2010; Nargund et al., 2012). Other key UPR^{mt} regulators include mitochondrial protease CLPP-1, mitochondrial matrix peptides exporter HAF-1, ubiquitin-like protein UBL-5, and transcription factor DVE-1 (Benedetti et al., 2006; Haynes et al., 2007; Haynes et al., 2010). Notably, the *atfs-1(gain of function)* mutant robustly activates *hsp-6p::gfp* (UPR^{mt} marker), yet fails to extend lifespan. This demonstrates that UPR^{mt} activation is necessary but insufficient for longevity (Bennett et al., 2014). Recent studies have extended these findings to mammals. Under ETC disruption, DELE1 is cleaved by OMA1 and activates HRI in the cytosol, triggering the mitochondrial integrated stress response (ISR^{mt}) via eIF2α phosphorylation (Fessler et al., 2020; Guo et al., 2020). Mitochondrial misfolding stress also activates UPR^{mt} through signals like mtROS and mitochondrial protein precursors via HSF-1 (Sutandy et al., 2023). Thus, mitochondrial stress response is an evolutionarily conserved pathway for cellular stress adaptation.

Mild mitochondrial stress during development has been shown to promote UPR^{mt} signaling and longevity by modifying chromatin status through epigenetic factors in *C. elegans*, including MET-2/LIN-65 complex, JMJD-3.1/3.2, NuRD complex, and CBP-1 (Li et al., 2021; Merkwirth et al., 2016; Shao et al., 2020; Tian et al., 2016; Zhu et al., 2020). Studies have

Citation: Zhou, J., Zhu, D., Wang, Y., Wang, Z., Zhang, N., Huang, X., Zhang, Y., Wang, Y., Wu, X., and Tian, Y. Mitochondrial stress orchestrates chromatin remodeling and longevity via phosphoregulation of the NuRD component LIN-40. Sci China Life Sci, https://doi.org/10.1007/s11427-025-2954-3

demonstrated that disruptions in oxidative phosphorylation (OXPHOS) lead to epigenetic remodeling, including histone acetylation, or chromatin condensation via the NuRD complex or MET-2/LIN-65 complex (Tian et al., 2016; Zhu et al., 2020). In fact, chromatin structure undergoes significant changes during aging; these modifications influence gene expression and may contribute to aging (Wu et al., 2024). Collectively, these findings suggest that mitochondria may serve as a central hub for aging signals, coordinating cellular and organismal aging via epigenetic remodeling and transcriptional control.

The NuRD complex is a highly conserved chromatin regulator involved in a wide array of biological processes, including embryonic development, maintenance of stem cell pluripotency, lineage specification, DNA damage response, tumorigenesis, stress adaptation, and aging (Pegoraro et al., 2009; Reid et al., 2023). The canonical NuRD complex comprises seven core components, including histone deacetylases (HDAC1/2), chromodomain helicase DNA-binding proteins (CHD3/4/5), retinoblastoma-binding proteins (RBBP4/7), GATAD2A/2B, the metastasis-associated proteins (MTA1/2/3), CDK2-associated protein (CDK2AP1/2), and methyl-CpG-binding domain protein (MBD2/3) (Reid et al., 2023). The NuRD complex fine-tunes gene expression by being selectively recruited to specific genomic loci through interactions with multiple regulatory elements. These include sequence-specific transcription factors, such as ZFP296, IKAROS, Thpok, Sall4 (Bottardi et al., 2014; Gao et al., 2022; Kloet et al., 2018; Wang et al., 2023), methyl-CpG-binding domain proteins MBD (*C. elegans* lacks canonical DNA methylation), and non-coding RNAs (Yu et al., 2024; Zhao et al., 2018). Through these mechanisms, NuRD modulates local chromatin accessibility and histone modification states, thereby enabling context-dependent regulation of transcription (Bornelöv et al., 2018; Reid et al., 2023).

Our previous research established a neuron-to-intestine mitochondrial stress model, in which neuronal WNT induced DVE-1::GFP accumulation in the intestinal nuclear in *C. elegans* (Li et al., 2022a; Zhang et al., 2018). Through a genetic screening approach, we identified several factors involved in inter-tissue regulation, including NuRD complex (Li et al., 2025; Li et al., 2022b; Liu et al., 2022; Wang et al., 2024; Zhu et al., 2020). Further investigations revealed that under mitochondrial stress, the mitochondrial metabolite acetyl-CoA cooperates with the NuRD complex to regulate chromatin remodeling, thereby promoting UPR^{mt} activation and contributing to lifespan extension. In this study, we further investigate the role of the NuRD complex in mitochondrial stress responses using mass spectrometry and protein modifications analysis. We showed that mitochondrial stress induces dephosphorylation of LIN-40 at the T654 site, which required p38 MAPK/PMK-3 kinase and PP1c/GSP-2 phosphatase. This dephosphorylation promotes chromatin condensation and UPR^{mt} activation, contributing to lifespan extension.

RESULTS

Mitochondrial stress triggers LIN-40 dephosphorylation to promote chromatin reorganization

The NuRD complex mediates mitochondrial stress-induced longevity through chromatin reorganization. However, the mechanism by which the NuRD complex responds to mitochondrial stress remains unclear. To explore this, we generated *lin-40::gfp* and *hda-1::mkate2::flag* knock-in *C. elegans* strains. We observed that LIN-40 and HDA-1 are broadly expressed across multiple cell types and localized within the nucleus (Figure S1A). As previously reported (Shao et al., 2020; Zhu et al., 2020), mitochondrial stress induced the accumulation of both LIN-40 and HDA-1 in the nucleus, the two components of NuRD complex (Figure S1B and C).

To identify the components of the NuRD complex responding to mitochondrial stress, we performed immunoprecipitation (IP) of LIN-40::GFP using GBP-Beads, followed by mass spectrometry (MS) analysis of *C. elegans* fed with either control RNAi (empty vector, EV) or *cco-1* RNAi to induce mitochondrial stress (Figure 1A). A wild-type strain N2 served as a control for non-specific protein bindings, and we excluded non-specific and ribosomal proteins from the LIN-40::GFP IP-MS results. We identified 305 proteins in control animals and 306 in *cco-1* RNAi-treated animals associated with LIN-40::GFP (Table S1). Among them, the NuRD core components were detected in both samples, and their scores were not significantly different (Figure 1B). Interestingly, MS data revealed multiple phosphorylation sites on LIN-40, including Thr151, Ser152, Ser153, Ser651, Thr654, Thr670, Thr744, Thr750, and Ser853. Notably, the phosphorylation intensity of T151S152S153 and S651T654 peptides decreased under *cco-1* RNAi-induced mitochondrial stress conditions (Figure 1C; Table S2). This suggests that mitochondrial stress induces significant dephosphorylation of LIN-40, which may be a key mechanism by which the NuRD complex mediates chromatin structure in response to mitochondrial stress.

Given our previous observation that intestinal nuclear size decreases in response to mitochondrial stress in a NuRD-dependent manner (Tian et al., 2016; Zhu et al., 2020), we tested the role of de-phosphorylation at the T151S152S153 or S651T654 sites in mitochondrial stress-induced chromatin condensation. We generated transgenic strains with mutations at these phosphorylation sites to mimic the non-phosphorylated (alanine, A) and continuously phosphorylated (aspartic acid, D) states, including *lin-40(T151A/S152A/S153A)*, *lin-40(T151D/S152D/S153D)*, *lin-40(S651A/T654A)*, and *lin-40(S651D/T654D)* fused with Flag::mCherry. These transgenes were introduced into the *lin-40*(*yth27*, G612E) mutant background, which is a loss-of-function allele we have identified from a genetic screen (Zhu et al., 2020).

We then measured the nuclear area in these animals with or without mitochondrial stress (induced by *cco-1* RNAi). Under normal conditions, none of the transgenic strains showed significant changes in nuclear size compared to wild-type (WT) animals (Figure S2A). However, under mitochondrial stress, the *lin-40(S651D/T654D)::Flag::mCherry* transgenic animals exhibited significantly enlarged intestinal nuclei compared to WT animals (Figure S2A). To determine whether both the S651 and T654 phosphorylation sites are required for mitochondrial stress-induced chromatin condensation, we generated transgenic strains *lin-40(T654D)::Flag::mCherry* and *lin-40(S651D)::Flag::mCherry*, and introduced these strains into *lin-40*(*yth27*) mutant. The LIN-40(T654D) mutation strongly attenuated chromatin condensation under mitochondrial stress, while the LIN-40 (S651D) mutation had no significant effect on chromatin structure compared to WT animals (Figure S2B).

To further validate the role of the T654 site, we used CRISPR/Cas9 technology to generate site-specific knock-in strains *lin-40*

https://doi.org/10.1007/s11427-025-2954-3

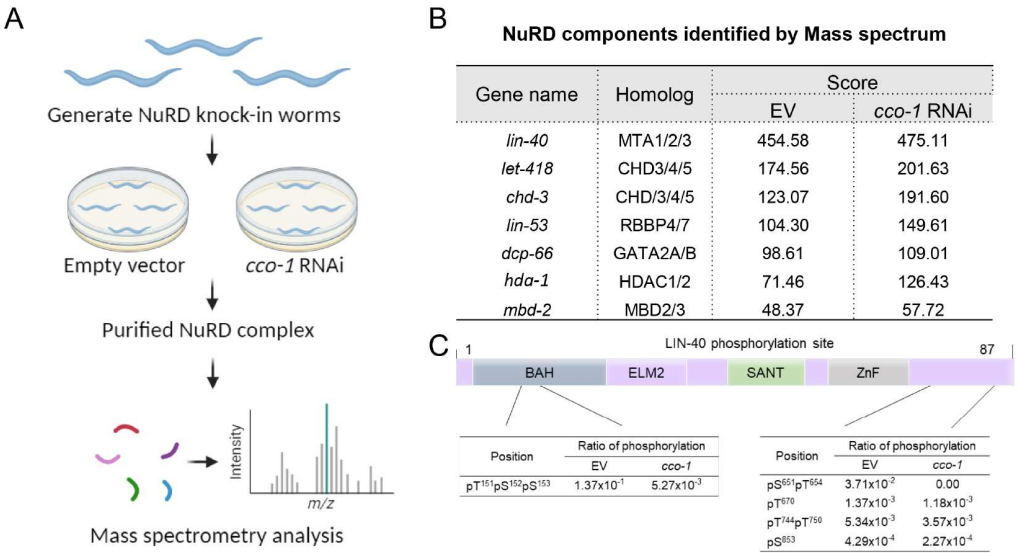

Figure 1. Mitochondrial stress induces dephosphorylation of MTA/LIN-40. A, The flow chart of mass spectrometry analysis of NuRD complex using *lin-40::gfp* knock-in worms grown on empty vector (EV) or *cco-1* RNAi bacteria. Created in BioRender. Wu, X. (2025) https://BioRender.com/yaoztnu. B, The table of NuRD components identified by mass spectrum. C, The ratio of the phosphorylation peptides of LIN-40 identified by mass spectrometry.

(T654D)::gfp and *lin-40(T654A)::gfp* (Figure S2C). Firstly, the T654 mutation did not affect LIN-40 protein levels, as shown by fluorescence imaging and Western blot analysis (Figure 2A–C). Consistent with our previous results, the *lin-40(T654D)::gfp* mutation significantly inhibited the chromatin condensation in response to *cco-1* RNAi treatment (Figure 2D and E). These findings demonstrate that chromatin changes induced by mitochondrial stress are strongly dependent on the phosphorylation status of LIN-40 at the T654 site.

Mitochondrial stress promotes UPR^{mt} via the LIN-40 T654 dephosphorylation

To investigate the role of LIN-40 pT654 phosphorylation site, we generated specific antibodies that recognize T654 using synthetic phosphorylated peptides, following established protocols (Figure S3A) (Arur and Schedl, 2014). These antibodies were first validated by dot blot analysis against control peptides (C-SNGTPASQ) and phosphorylated peptides (C-SNG(T-p)PASQ). Three of them demonstrated good specificity, including E17547P, E17549P, and E17920P. We selected E17547P for further analysis (Figure S3B). These antibodies successfully detected LIN-40 proteins but did not recognize the LIN-40 (T654A) and LIN-40(T654D) mutant proteins (Figure 3A). We further validated the phosphorylation status of LIN-40::GFP under various ETC components RNAi treatment using GBP-Beads for purification, followed by Western blotting with the Lin-40(pT654) antibody (Figure 3B and C). The phosphorylation levels at T654 significantly decreased under mitochondrial stress, confirming our IP-MS findings that T654 dephosphorylate occurs in response to mitochondrial dysfunction.

The NuRD complex is evolutionarily conserved and regulates gene expression primarily through histone deacetylation and nucleosome remodeling. Transcription factors often guide the NuRD complex to specific genomic target sites. Based on this, we hypothesized that the phosphorylation status of LIN-40 at the T654 site might modulate its interaction with transcription factors, potentially influencing NuRD complex function under stress.

Previous studies have shown that the NuRD complex interacts with the transcription factor DVE-1; however, which component directly interacts with DVE-1 remains unclear. By using a bioinformatics approach, we predicted that HDA-1 might directly interact with DVE-1. We expressed and purified HDA-1 and DVE-1 proteins in vitro to test this. Pull-down assays confirmed a direct interaction between HDA-1 and DVE-1 (Figure 3D).

Next, we purified the NuRD complex using the strain containing both *lin-40::gfp KI* and *hda-1::Flag::mkate2 KI* with GBP-beads. We then examined DVE-1 and HDA-1 protein levels in the complex using a DVE-1 endogenous antibody we generated previously (Zhu et al., 2020) and FLAG antibody, respectively. Co-IP experiments revealed that LIN-40(T654D) mutant protein exhibited a reduced binding affinity for DVE-1 or HDA-1 protein compared to wild-type LIN-40 (Figure 3E–G). These results suggest that the LIN-40 T654 dephosphorylation affects NuRD complex assembly and its interaction with DVE-1, which may guide the complex to specific target sites under mitochondrial stress.

To explore whether the LIN-40 T654 dephosphorylation is required for the expression of mitochondrial stress response genes, we used qPCR to measure the expression levels of *hsp-6*, *hsp-60*, *lonp-1*, and *ymel-1*. Our data showed that the *lin-40 (T654D)* mutation significantly inhibited the upregulation of these genes under mitochondrial stress (Figure 3H–K).

Our previous research demonstrated that LIN-40 is essential for the nuclear accumulation of DVE-1-GFP in response to mitochondrial stress (Tian et al., 2016; Zhu et al., 2020). Therefore, we investigated the effect of the T654D phosphomimetic mutation on DVE-1-GFP nuclear localization. The results showed that the T654D mutation significantly impairs the accumulation of DVE-1 in the nucleus under *cco-1* RNAi (Figure 3L and M).

In summary, our findings demonstrate that mitochondrial stress drives LIN-40 T654 dephosphorylation, which facilitates

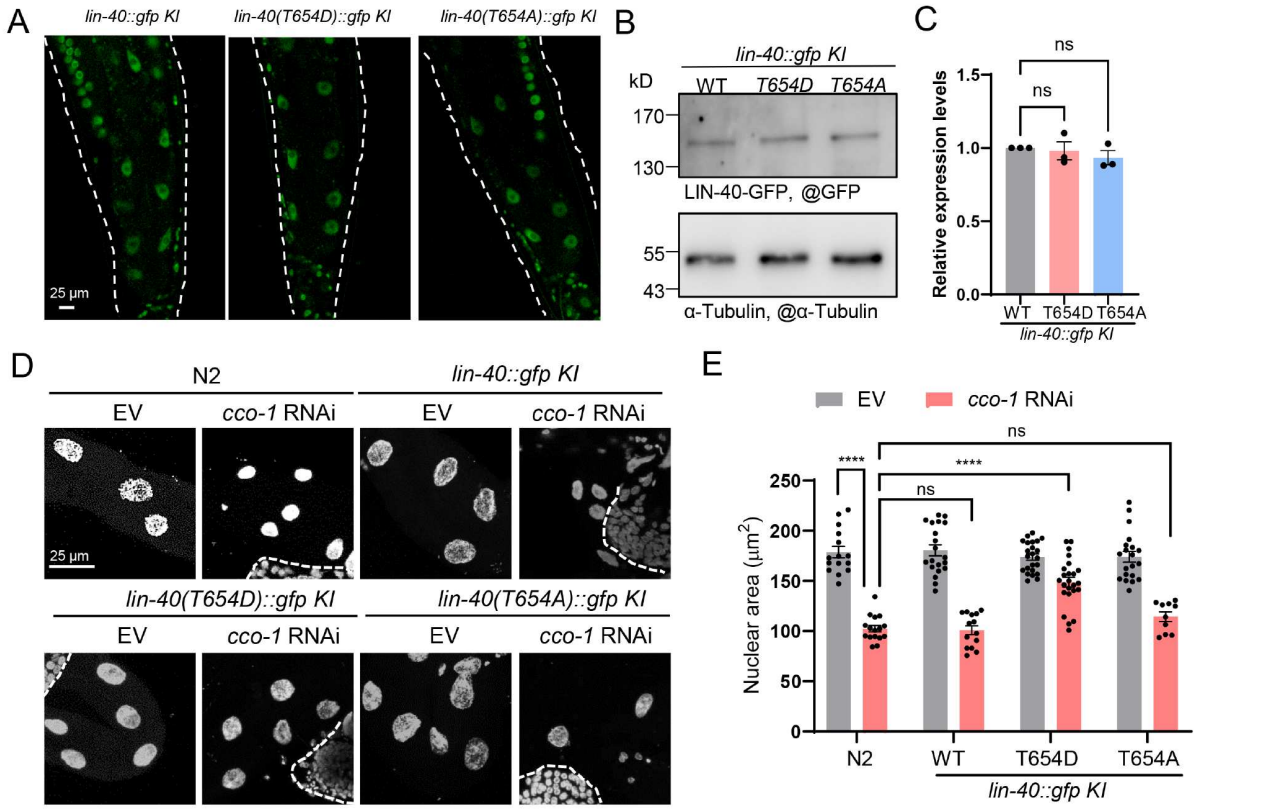

Figure 2. Mitochondrial stress induces MTA/LIN-40 dephosphorylation to facilitate chromatin remodeling. A, Representative photomicrographs of *lin-40::gfp KI*, *lin-40 (T654D)::gfp KI* and *lin-40(T654A)::gfp KI animals*. Scale bar=25 μm. B, Immunoblots of GFP and Tubulin in *lin-40::gfp KI*, *lin-40(T654D)::gfp KI* and *lin-40(T654A)::gfp KI* animals at day 1 stage. C, Quantification of relative expression levels of GFP (relative to Tubulin) in *lin-40::gfp KI*, *lin-40(T654D)::gfp KI* and *lin-40(T654A)::gfp KI* animals as depicted in (B). n=3. ns denotes P>0.05 via one-way ANOVA followed by Tukey's test (paired). Error bars represent ±SEM. D, Representative maximal intensity projection images of DAPI immunostaining of intestinal nuclei of *lin-40::gfp KI*, *lin-40(T654D)::gfp KI* and *lin-40(T654A)::gfp KI* animals at day 1 stage that grown on EV or *cco-1* RNAi bacteria. Scale bar=25 μm. E, Quantification of the intestinal nuclear area as shown in (D). $n \geqslant 10$ nuclei. **** P<0.0001 and ns denotes P>0.05 via two-way ANOVA followed by Tukey's test. Error bars represent ±SEM.

NuRD complex assembly, and it is associated with DVE-1, leading to the activation of UPR^{mt} signaling.

p38 MAPK/PMK-3 regulates the phosphorylation status of LIN-40

Previous studies found that the mammalian homolog of LIN-40, MTA1, is phosphorylated by protein kinase D1 (PKD1), which inhibits its nuclear localization and promotes degradation (Ganju et al., 2018). Since *C. elegans* lacks a PKD1 homolog, we used PhosphoSitePlus, a protein phosphorylation site prediction tool, to identify potential kinases for LIN-40 T654 (Hornbeck et al., 2015). This analysis revealed that the peptide $_{652}$NGTPA$_{657}$ is a predicted substrate for both the p38 mitogen-activated protein kinase (MAPK) family and cyclin-dependent kinase (CDK) family (Figure S4A). To identify the kinase responsible for phosphorylating LIN-40 at T654, we conducted a small-scale RNAi screen targeting the predicted kinases using LIN-40::Flag::mCherry animals. Our screen revealed that PMK-3, a member of the p38 MAPK subfamily, plays a role in the nuclear accumulation of LIN-40 (Figure S4B; Figure 4A and B).

To validate the interaction between LIN-40 and PMK-3, we performed an in vivo co-immunoprecipitation assay using *lin-40::gfp KI* animals co-expressing *pmk-3::mCherry::HA*. This assay confirmed that PMK-3 interacts with LIN-40 (Figure 4C). To assess whether PMK-3 regulates the phosphorylation of LIN-40 at T654, we examined T654 phosphorylation levels in *lin-40::gfp KI* animals carrying the *pmk-3(ok169)* mutation. As PMK-3 is a putative kinase for LIN-40, we hypothesized that its loss would reduce LIN-40 T654 phosphorylation. Consistent with this, T654 phosphorylation was significantly reduced in *pmk-3 (ok169)* mutants compared to wild-type animals (Figure 4D and E). These findings indicate that p38 MAPK/PMK-3 is required for LIN-40 T654 phosphorylation.

However, the size of intestinal nuclei in *pmk-3(ok169)* mutants remained similar to those in WT animals (Figure S4C and D), and the PMK-3 protein levels did not change under mitochondrial stress, as shown by fluorescence imaging (Figure S4E). While dephosphorylation of LIN-40 at T654 is critical for chromatin remodeling in response to mitochondrial stress, the size of intestinal nuclei in lin-40(T654A)::gfp worms remained similar with WT animals (Figure 2D and E), and these results suggest that it may not be sufficient on its own to drive chromatin remodeling, implicating additional regulatory mechanisms.

Phosphatase PP1c/GSP-2 mediates LIN-40 dephosphorylation

Protein phosphorylation is dynamically regulated by both kinases and phosphatase. In *C. elegans*, there are 244 predicted

https://doi.org/10.1007/s11427-025-2954-3

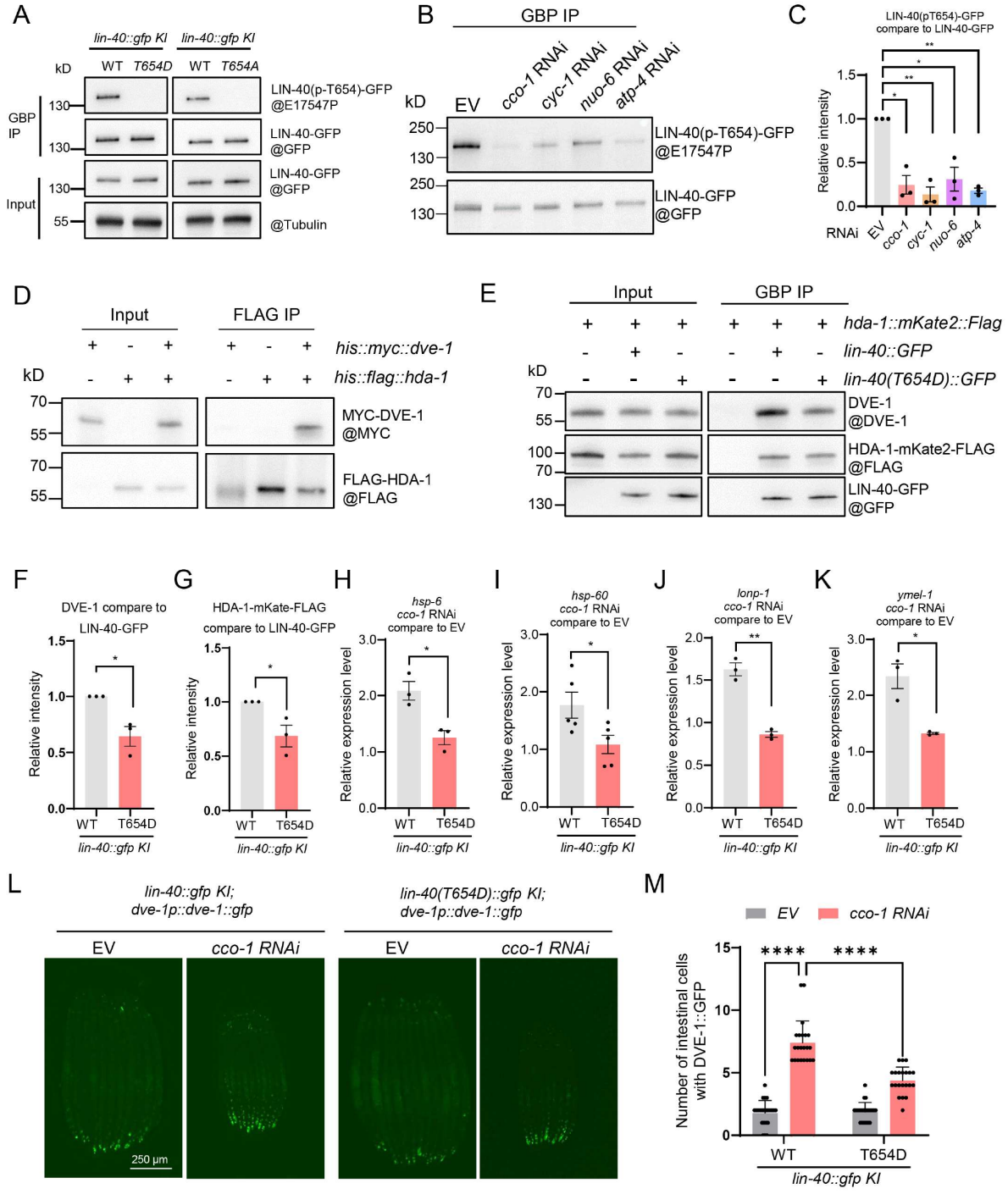

Figure 3. LIN-40 T654 site dephosphorylation regulates UPR^{mt} activation. A, Immunoblots of LIN-40(p-T654), GFP and Tubulin in GBP immunoprecipitation or input fractions of *lin-40(WT)::gfp KI*, *lin-40(T654A)::gfp KI* or *lin-40(T654D)::gfp KI* animals. B, Immunoblots of LIN-40(p-T654) and GFP in GBP immunoprecipitation fractions of *lin-40::gfp KI* animals at YA stage that grown on EV, *cco-1*, *cyc-1*, *nuo-6* or *atp-4* RNAi bacteria. C, Quantification of the mean intensity of LIN-40(p-T654)-GFP relative to LIN-40-GFP intensity in animals as shown in (B). n=3. *P<0.05, **P<0.01 via paired two-tailed Student's t test. Error bars represent ±SEM. D, Immunoblots of MYC and FLAG in input or FLAG immunoprecipitation fractions. E, Immunoblots of DVE-1, FLAG and GFP in GBP immunoprecipitation or input fractions of *hda-1::mKate2::Flag KI*, *hda-1::mKate2::Flag KI*; *lin-40::gfp KI*, or *hda-1::mKate2::Flag*; *lin-40(T654D)::gfp KI* animals at YA stage. F, Quantification of the mean intensity of DVE-1 relative to LIN-40-GFP intensity in animals as shown in (E). n=3. *P<0.05 via paired two-tailed Student's t test. Error bars represent ±SEM. G, Quantification of the mean intensity of HDA-1::mKate2::FLAG relative to LIN-40-GFP intensity in animals as shown in (E). n=3. *P<0.05 via paired two-tailed Student's t test. Error bars represent ±SEM. H, Quantitative PCR of *hsp-6* mRNA level in synchronized L4 worms with *lin-40(WT)::gfp KI* or *lin-40(T654D)::gfp KI* background grown on *cco-1* RNAi bacteria compared to EV. n=3. I, Quantitative PCR of *hsp-60* mRNA level in synchronized L4 worms with *lin-40(WT)::gfp KI* or *lin-40(T654D)::gfp KI* background grown on *cco-1* RNAi bacteria compared to EV. n=5. J, Quantitative PCR of *lonp-1* mRNA level in synchronized L4 worms with *lin-40(WT)::gfp KI* or *lin-40(T654D)::gfp KI* background grown on *cco-1* RNAi bacteria compared to EV. n=3. K, Quantitative PCR of *ymel-1* mRNA level in synchronized L4 worms with *lin-40(WT)::gfp KI* or *lin-40(T654D)::gfp KI* background grown on *cco-1* RNAi bacteria compared to EV. n=3. *P<0.05, **P<0.01 via paired two-tailed Student's t test. Error bars represent ±SEM. L, Representative fluorescence images of DVE-1::GFP. Animals were raised on EV or *cco-1* RNAi from hatching, and images were taken at day 1 of adulthood. Genotypes are indicated above each image. Scale bar=250 μm. M, Quantification of the number of intestinal cells with strong GFP signal in animals as depicted in (L). n≥21. ****P<0.0001 via two-way ANOVA followed by Tukey's test. Error bars represent ±SEM.

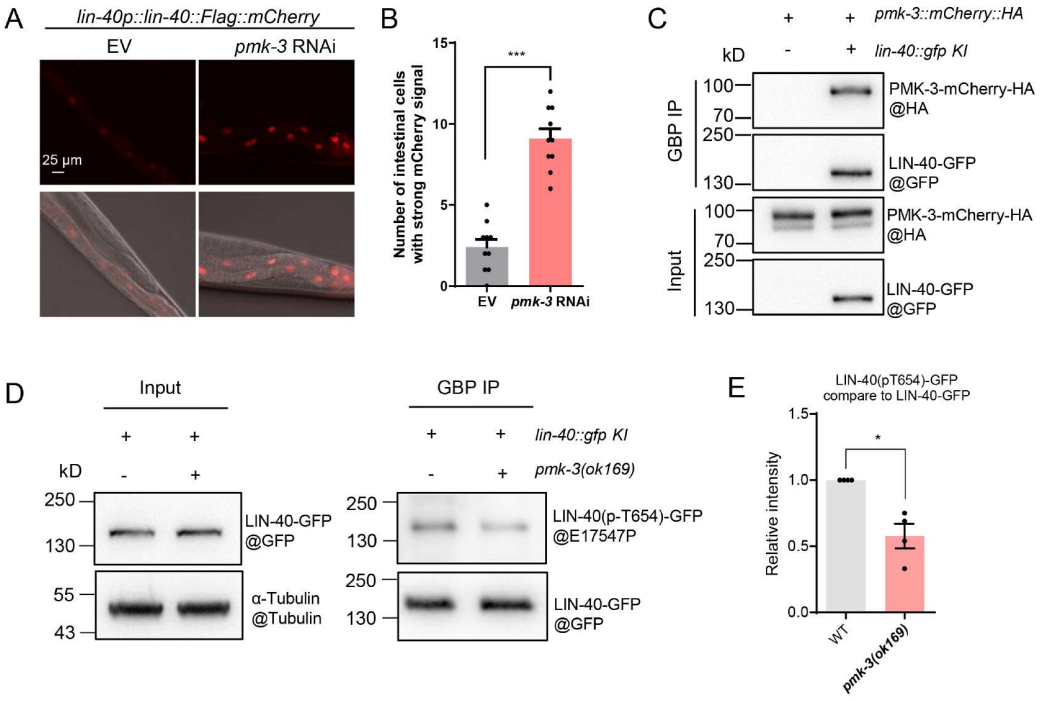

Figure 4. PMK-3 kinase mediates LIN-40 T654 phosphorylation. A, Representative photomicrographs of *lin-40p::lin-40::Flag::mCherry* grown on EV and *pmk-3* RNAi bacteria. Scale bar=25 μm. B, Quantification of the number of intestinal cells with strong mCherry signal in animals as depicted in (A). n=10. ***P<0.001 via unpaired two-tailed Student's t test. Error bars represent ±SEM. C, Immunoblots of HA, GFP in GBP immunoprecipitation or input fractions of *pmk-3::mCherry:HA* and *pmk-3::mCherry:HA*; *lin-40::gfp KI* animals at YA stage. D, Immunoblots of GFP, Tubulin and LIN-40(p-T654) in GBP immunoprecipitation or input fractions of *lin-40::gfp KI* and *lin-40::gfp KI*;*pmk-3(ok169)* animals at YA stage. E, Quantification of the intensity of LIN-40(p-T654) relative to GFP in GBP immunoprecipitation fraction of animals as depicted in (D). n=4. *P<0.05 via paired two-tailed Student's t test. Error bars represent ±SEM.

protein phosphatases (Chen et al., 2017). To investigate the mechanism underlying mitochondrial stress-induced dephosphorylation of LIN-40 at T654, we analyzed the results of our LIN-40::GFP IP-MS experiment. From this analysis, we identified four phosphatases interacting with LIN-40, including PP1c/GSP-2, PP2a/LET-92, and PPM-1.A and PPM-1.G (Figure S5A). Given that LIN-40::Flag::mCherry accumulates in intestinal nuclei under mitochondrial stress when fed *cco-1* RNAi bacteria, we performed a small-scale RNAi screening targeting these four phosphatases using LIN-40::Flag::mCherry animals (Figure S5B). Our screen revealed that PP1c/GSP-2 is involved in the nuclear accumulation of LIN-40 during mitochondrial stress (Figure 5A and B).

We performed a GST pull-down assay to investigate the interaction between GSP-2 and LIN-40. This experiment demonstrated that GST::GSP-2 directly binds to LIN-40::Flag::mCherry (Figure 5C). Additionally, fluorescence imaging revealed that GSP-2 protein levels remain unchanged under mitochondrial stress (Figure S5C).

To determine whether GSP-2 regulates the dephosphorylation of LIN-40 at T654, we analyzed the phosphorylation levels of LIN-40 T654 under mitochondrial stress in *gsp-2* knockdown animals using a phosphorylation-specific antibody. Immunoblots from *lin-40::gfp KI* animals showed that LIN-40 pT654 phosphorylation remained elevated in *gsp-2* RNAi knockdown animals under mitochondrial stress, whereas phosphorylation levels decreased in control animals (Figure 5D and E).

Furthermore, we examined chromatin structure in *gsp-2* knockdown animals. Under normal conditions, *gsp-2* knockdown had no effect on chromatin organization. However, under mitochondrial stress induced by *cco-1* RNAi, *gsp-2* knockdown significantly impaired chromatin condensation, in contrast to control animals, where chromatin condensation occurred (Figure 5F and G).

Based on our previous findings that phosphorylation at the T654 site influences the nuclear accumulation of DVE-1 in response to mitochondrial stress, we further analyzed the localization of DVE-1-GFP in intestinal cells. Animals were fed with EV, EV+*cco-1* RNAi, EV+*gsp-2* RNAi, or *cco-1*+*gsp-2* RNAi bacteria from hatch. We analyzed the fluorescence intensity of DVE-1-GFP in intestinal nuclei on day 1. The results showed that EV+*cco-1* RNAi induced DVE-1 nuclear accumulation in the intestine, while *gsp-2* RNAi significantly suppressed this accumulation (Figure 5H and I).

These findings indicate that GSP-2 mediates the dephosphorylation of LIN-40 at T654 and is essential for chromatin condensation and DVE-1 accumulation in response to mitochondrial stress.

The phosphorylation status of LIN-40 T654 is essential for mitochondrial stress-induced longevity

Mitochondrial stress during development is known to extend lifespan in *C. elegans* via the NuRD complex. To investigate the role of the LIN-40 T654 phosphorylation in this process, we analyzed the lifespan of *lin-40(T654D)* (phospho-mimetic) and *lin-40(T654A)* (phospho-null) mutant animals, with or without *cco-1* RNAi treatment.

Under normal conditions, the lifespan of *lin-40(T654D)* mutants was comparable to WT animals. However, when

https://doi.org/10.1007/s11427-025-2954-3

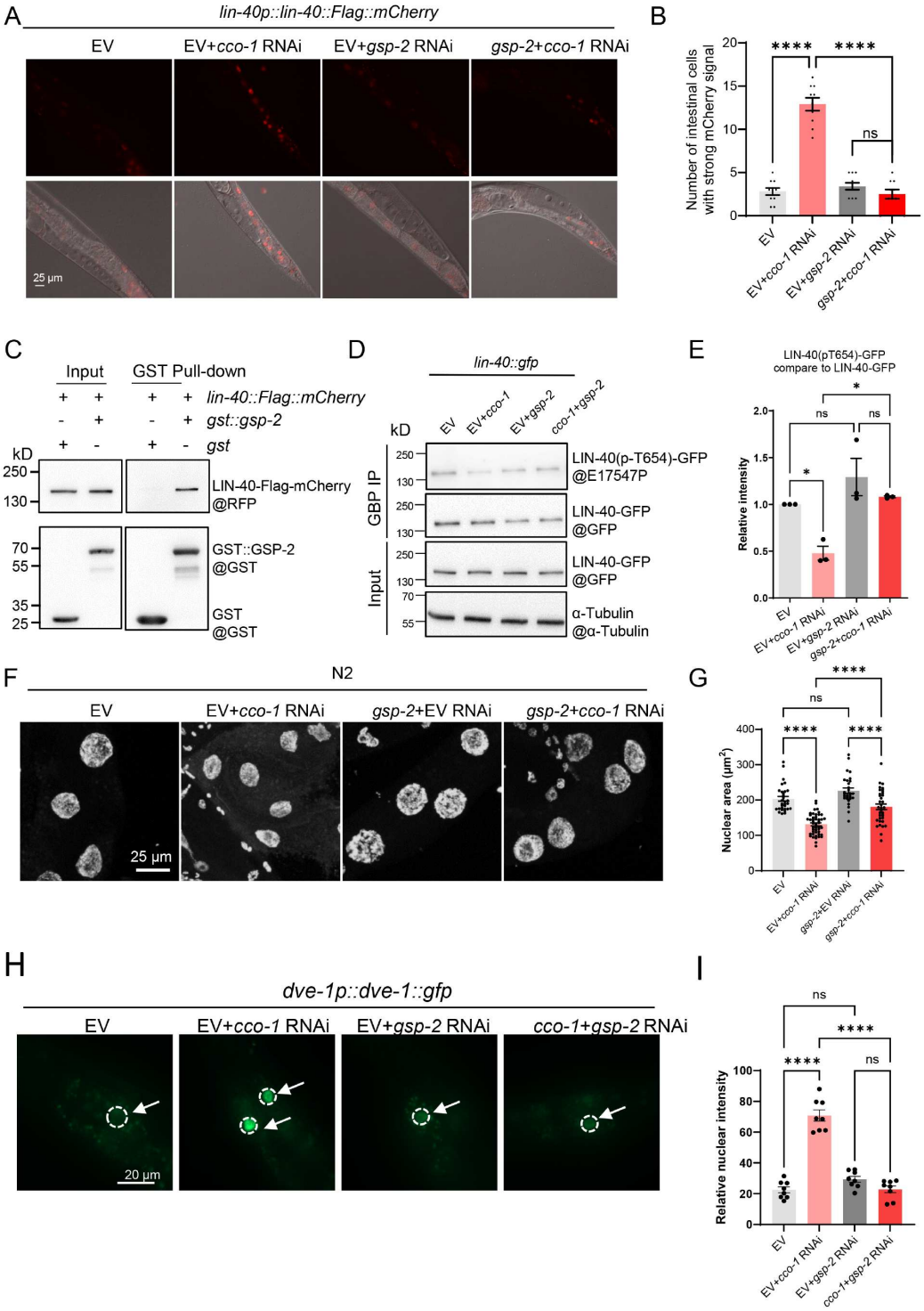

Figure 5. GSP-2 phosphatase mediates LIN-40 T654 dephosphorylation. A, Representative photomicrographs of *lin-40p::lin-40::Flag::mCherry* animals at day 1 stage that grown on empty vector (EV), EV+*cco-1*, EV+*gsp-2* or *gsp-2*+*cco-1* RNAi bacteria. Scale bar=25 μm. B, Quantification of the number of intestinal cells with strong mCherry signal in animals as depicted in (A). n=10. ****P<0.0001 and ns denotes P>0.05 via one-way ANOVA followed by Tukey's test (unpaired). Error bars represent ±SEM. C, Immunoblots of RFP and GST in input fractions and GST pull-down fractions of LIN-40::FLAG::mCherry incubated with GST or GST::GSP-2, as indicated. D, Immunoblots of LIN-40(p-T654) and GFP in GBP immunoprecipitation or input fractions of *lin-40::gfp KI* animals at YA stage that grown on EV, EV+*cco-1*, EV+*gsp-2* or *gsp-2*+*cco-1* RNAi bacteria, as indicated. E, Quantification of the intensity of LIN-40(p-T654)-GFP relative to LIN-40-GFP in GBP IP fractions of animals as depicted in (D). n=3. *P<0.05 and ns denotes P>0.05 via one-way ANOVA followed by Tukey's test (paired). Error bars represent ±SEM. F, Representative maximal intensity projection images of DAPI immunostaining of intestinal nuclei of N2 animals at day 1 stage that grown on EV, EV+*cco-1* RNAi, EV+*gsp-2* or *gsp-2*+*cco-1* RNAi bacteria. Scale bar=25 μm. G, Quantification of the intestinal nuclear maximum cross-section area at day 1 stage in animals as shown in (F). $n \geq 29$ nuclei. ****P<0.0001 and ns denotes P>0.05 via one-way ANOVA followed by Tukey's test (unpaired). Error bars represent ±SEM. H, Representative photomicrographs of *dve-1p::dve-1::gfp* animals at day 1 stage that grown on EV, EV+*cco-1*, EV+*gsp-2* or *gsp-2*+*cco-1* RNAi bacteria. Scale bar=25 μm. I, Quantification of DVE-1-GFP intensity localized in intestinal nuclei (near the head region) of day 1 adult animals, as shown in (H). n=8. ****P<0.0001 and ns denotes P>0.05 via one-way ANOVA followed by Tukey's test (unpaired). Error bars represent ±SEM.

subjected to mitochondrial stress, *lin-40(T654D)* animals displayed a partial but consistent suppression of lifespan extension. These results suggest that LIN-40 T654 dephosphorylation is crucial for mediating mitochondrial stress-induced longevity (Figure 6A). In contrast, *lin-40(T654A)* mutants exhibited a lifespan similar to WT animals under both normal and mitochondrial stress conditions, indicating that the loss of phosphorylation alone does not affect lifespan (Figure 6B).

We also examined changes in mitochondrial morphology using intestinal-specific mitochondrial reporter *ges-1p::tomm-20::mKate2::HA*(Ahier et al., 2018). The results showed that under *cco-1* RNAi conditions, intestinal mitochondria appeared more fragmented, smaller, and failed to form a network compared to those under EV control (Figure 6C). This fragmented mitochondrial phenotype was consistently observed across all three genetic backgrounds analyzed. We also measured mitochondrial respiration and found that *cco-1* RNAi significantly reduced the oxygen consumption rate (OCR), but there were no notable differences among the different genotypes (Figure S6A, Table S3). Previous studies have shown that mitochondrial dysfunction during development can lead to reduced body size and decreased brood size. To assess whether LIN-40 T654 mutations influence these developmental outcomes, we examined body size and progeny number across genotypes and found no significant differences (Figure S6B and C). Overall, the T654 phosphorylation-related mutation of LIN-40 does not appear to affect mitochondrial morphology or function at day 1 of adulthood, nor does it influence the development or reproduction of *C. elegans*. Instead, it exerts long-term effects and contributes to mitochondrial-to-nuclear communication and lifespan extension under mitochondrial stress conditions.

Overall, these findings reveal that mitochondrial stress induces dephosphorylation at the T654 site of LIN-40/MTA, a process that depends on both kinase PMK-3 and phosphatase GSP-2. Furthermore, phosphorylation at this site is essential for mitochondrial stress-induced UPR^{mt} activation, chromatin remodeling, and the promotion of longevity (Figure 6D).

DISCUSSION

Mitochondria-nuclear communication plays a crucial role in regulating the aging process. Through metabolites, transcription factors, and epigenetic modifications, mitochondria influence the expression of nuclear genes to enable cellular adaptation to environmental stress. However, the mechanisms by which epigenetic factors respond to mitochondrial stress remain poorly understood. Here, we discovered that the NuRD complex component MTA/LIN-40 undergoes dephosphorylated in response to mitochondrial stress, a modification that regulates chromatin condensation, activates the UPR^{mt}, and promotes lifespan extension.

The NuRD complex is a conserved epigenetic regulator involved in diverse biological processes, including development, differentiation, disease progression, and aging (Basta and Rauchman, 2015; Lai and Wade, 2011). During aging, the function of NuRD complex components declines, contributing to chromatin defects and aging-associated phenotypes (Pegoraro et al., 2009). In *C. elegans*, mutation in *lin-40* or *lin-53*, the key NuRD components, leads to a shortened lifespan (De Vaux et al., 2013; Zhu et al., 2020; Zimmerman and Kim, 2014). Given that aging is associated with global chromatin alterations, such as heterochromatin loss and histone modification changes, our findings suggest that mitochondrial regulation of the NuRD complex and its associated chromatin remodeling activity is a crucial aspect of the aging process and worth further investigation.

Phosphorylation is a dynamic and reversible post-translational modification that plays an essential role in cellular signaling. While phosphoproteomics studies have identified phosphorylation sites on NuRD components, the physiological relevance of these modifications in response to stress or aging remains largely unexplored (Bouazoune and Brehm, 2005; Polo et al., 2010; Sun et al., 2007). Similar phosphorylation events have been described in mammalian systems; for instance, MTA1 phosphorylation by PKD1 promotes its degradation and inhibits tumor growth (Ganju et al., 2018). Our findings extend these observations by demonstrating a functional role for LIN-40 phosphorylation in regulating chromatin remodeling and lifespan in response to mitochondrial stress. These insights could inform future research into the role of MTA family proteins in aging and stress responses in higher organisms.

Protein phosphatase 1 (PP1) is a conserved serine/threonine phosphatase that functions in conjunction with regulatory subunits to govern diverse biological processes. Dysregulated PP1 activity has been implicated in developmental abnormalities, tumorigenesis, and aging (Genoux et al., 2002; Xing et al., 2023). Our study identifies PP1c/GSP-2 as a critical regulator of LIN-40 dephosphorylation in response to mitochondrial stress. These findings suggest a broader role for PP1 in regulating epigenetic responses to stress and highlight its potential as a therapeutic target for aging-related interventions.

In summary, our work reveals a phosphorylation-dependent mechanism by which the NuRD complex component LIN-40 mediates mitochondrial stress responses, linking epigenetic regulation to lifespan extension. These findings provide a foundation for future studies investigating how mitochondrial signals influence chromatin dynamics and aging, with potential implications for understanding epigenetic regulation in higher organisms.

MATERIALS AND METHODS

Worm strains and maintenance

Nematodes *C. elegans* were maintained as previously described (Brenner, 1974). Worms were grown at 20°C on a standard nematode growth medium (NGM) agar plates seeded with *Escherichia coli* OP50 or HT115. OP50 was cultured overnight in LB at 37°C. HT115 was used to perform RNAi and was cultured overnight at 37°C in LB containing carbenicillin (Inalcopharm, USA) (100 μg mL^{-1}). Strains used in this study were listed in Table S4.

Transgenic strain construction

The *lin-40* 2-kb promoter, *lin-40* cDNA, Flag sequence and mCherry sequence were used to generate *lin-40p::lin-40::flag::mCherry* transgenic strain. Based on this construct, ST-AA transgenic construct was mutagenized in Ser651Tyr654 to Ala65Ala654, respectively. ST-DD transgenic construct was mutagenized in Ser651Tyr654 to Asp651Asp654, respectively. TSS-AAA transgenic construct was mutagenized in Tyr151-Ser152Ser153 to Ala151Ala152Ala153, respectively. TSS-DDD

https://doi.org/10.1007/s11427-025-2954-3

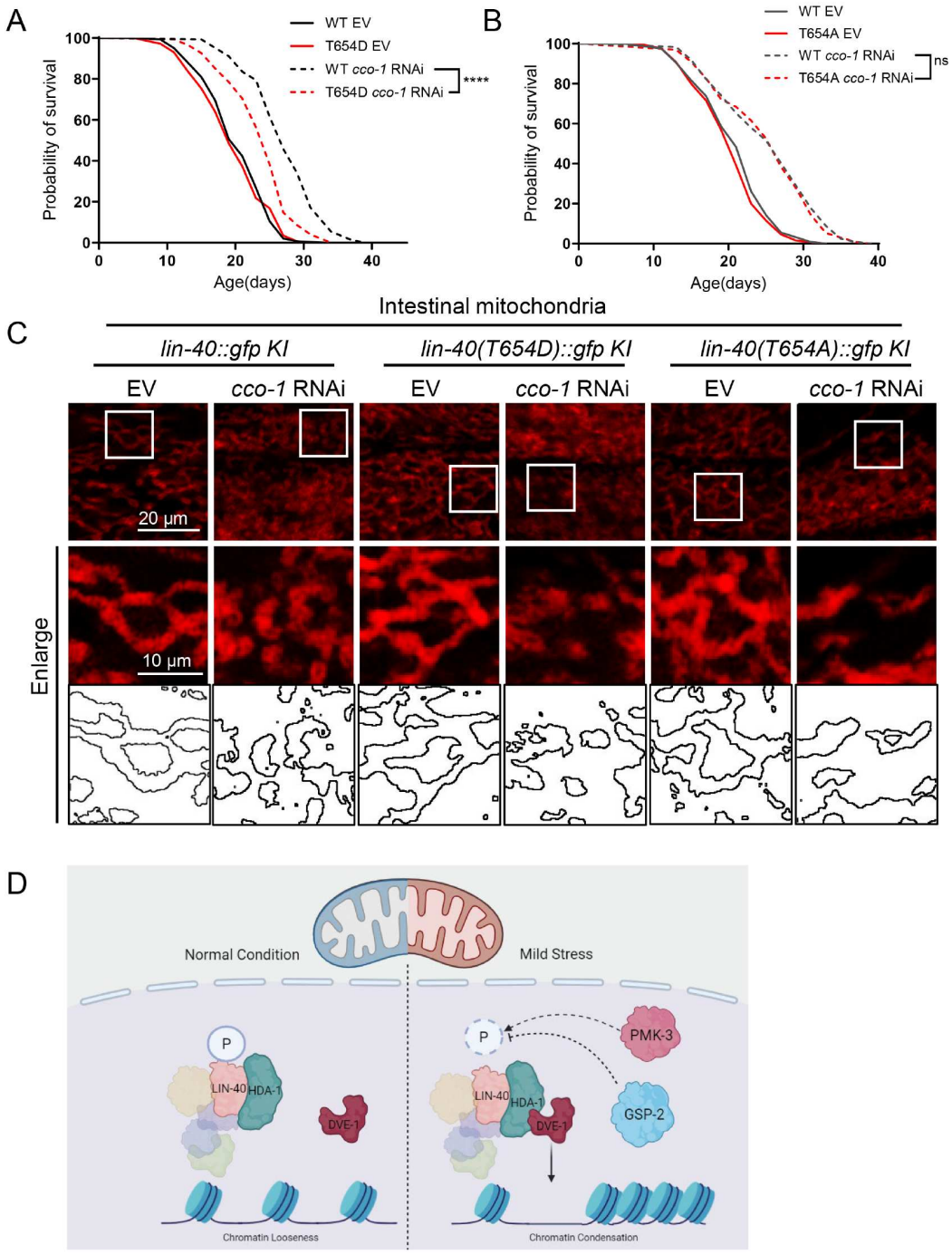

Figure 6. LIN-40 T654 phosphorylation modulates mitochondrial stress-induced lifespan extension. A, Survival analyses of *lin-40::gfp KI* and *lin-40(T654D)::gfp KI* animals that grown on EV or *cco-1* RNAi bacteria. ****P<0.0001 via Log-rank (Mantel-Cox) test. B, Survival analyses of *lin-40::gfp KI* and *lin-40(T654A)::gfp KI* grown on EV or *cco-1* RNAi bacteria. ns denotes P>0.05 via Log-rank (Mantel-Cox) test. C, Representative images of mitochondrial networks in intestinal cells of day 1 adult animals grown on EV or *cco-1* RNAi, as indicated. Genotypes are labeled above each image. The bottom panel shows enlarged views highlighting mitochondrial morphology. D, The model of LIN-40 sensing mitochondrial stress via phosphorylation of T654, which depended on phosphatase GSP-2 and the kinase PMK-3. Created in BioRender. Wu, X. (2025) https://BioRender.com/va2prss.

transgenic construct was mutagenized in Tyr151Ser152Ser153 to Asp151Asp152Asp153, respectively. S651D transgenic construct was mutagenized in Ser651 to Asp651. T654D transgenic construct was mutagenized in Tyr654 to Asp654.

The *gsp-2* 2-kb promoter and *gsp-2* cDNA were used to generate *gsp-2p::gsp-2::mCherry*; the *pmk-3* 2-kb promoter and 3.5-kb *pmk-3* genomic DNA, including 5′UTR and first intron, were used to generate *pmk-3p::pmk-3::mCherry::HA*.

CRISPR Cas9 gene editing

PHX2447: syb2447[hda-1::mKate2::Flag] and PHX2115: syb2115[lin-40::gfp] were generated by SunyBiotech (http://www.sunybiotech.com/) using CRISPR-Cas9. To generate *lin-*

40::gfp KI worm, GFP coding sequence was inserted into C-terminus of *lin-40* as "cacatttttttgcagAAC(gfp)TAAacgacggaacctactcactcgtc".

To generate *hda-1::mKate2::Flag KI* worm, mKate2 and Flag sequences were inserted into the C-terminus of *hda-1* as "AGCGTCAGAAGACAGAG(mKate2-flag) TAAaacactaaaatgtgcc".

LTY2362: yth102[lin-40(T654D)::gfp] and LTY2359: yth99 [lin-40(T654A)::gfp] were generated by our lab using CRISPR-Cas9 as indicated in Figure S2C.

RNAi feeding

Age-synchronized worms were bleached and grown from hatch on *E. coli* HT115 strains containing an empty vector control or double-stranded RNA. RNAi strains were from the Vidal library or the Ahringer library.

Microscopy and image analysis

Analysis of the fluorescence intensity in whole worm

For whole-animal fluorescence image, worms were anesthetized with 10 mmol L^{-1} potassium azide (Macklin, Shanghai, China). For *lin-40p::lin-40::Flag::mCherry*, *pmk-3p::pmk-3::mCherry*, and *gsp-2p::gsp-2::mCherry* imaging, we use Zeiss Imager M2 microscope or Leica M165 FC dissecting microscope for the same set of experiments with the same parameters.

For *lin-40::gfp KI*, *lin-40(T654D)::gfp KI*, *lin-40(T654A)::gfp KI* and *hda-1::mKate2::Flag* imaging, we use Leica-TCS SP8, laser scanning confocal microscope, for the same set of experiments with the same parameters.

For mitochondrial morphology analysis, we use Zeiss LSM 980 confocal microscope with Airyscan for the same set of experiments with the same parameters.

Dissection and fixation for intestinal nuclei analysis

Dissection and fixation were carried out by a modified freezing-crack method. Worms were dissected in M9 buffer on a poly-lysine-coated slide. The slides were fixed in methanol for 10 min, followed by acetone for 10 min at −20°C. Next, the slides were placed in phosphate-buffered saline (PBS) and washed with fresh PBS for 5 min. Slides were then mounted with 4′,6-diamidino-2-phenylindol (DAPI) solution (Vector laboratories, USA).

Maximum cross-section area analysis of intestinal nuclei

Intestinal cells were imaged at ×63 magnification using Leica-TCS SP8, laser scanning confocal microscope. Z-stacks of the intestinal nuclei were analyzed using LAS X. Contours of individual nuclei, according to DAPI fluorescence, were manually defined and used to render nuclei area. The maximum cross-sectional area of each nucleus was acquired from the surface tool statistics by ImageJ 1.54P.

RNA extraction and qPCR analysis

Total RNA was isolated using TRIzol (Invitrogen, USA). Worms were synchronized and washed off the plates using M9 buffer, and 1 mL TRIzol was added to the samples and homogenized by repeated freezing and thawing using liquid nitrogen. RNA was isolated according to the manufacturer's instructions. DNA was wiped off using RQ1 RNase-Free DNase (Promega, USA). cDNA was synthesized using the M-MLV Reverse Transcriptase (Invitrogen). Gene expression levels were determined by real-time PCR using SYBR Green Real-time PCR Master Mix (Toyobo, Japan) and Bio-rad CFX96 Real-Time PCR Detection Systems. Relative gene expression was normalized to *act-3* (T04C12.4) mRNA levels. Fold changes in gene expression were calculated using the comparative ΔΔCt method, and then normalized to the control for every single biological repeat. The primer sequences used in the quantitative PCR are shown in Table S5. For each experiment, more than three biological samples were analyzed.

Liquid culture

In this study, experiments involving protein purification required a large number of worms, and we used liquid culture, which is from wormbook, to obtain sufficient experimental material for all of them. All the chemical reagents are from Sigma (USA).

Add 50 mL S-Medium to a sterilized 250 mL flask. Inoculate the S-Medium with a concentrated *E. coli* OP50 or corresponding RNAi HT115 from 1 L of an overnight culture. Worms were synchronized for liquid culture. Put the flask in a shaker at 20°C, 200 r min^{-1}.

S-Medium was prepared as described in the wormbook. 1 L S Basal (5.85 g NaCl, 1 g K_2HPO_4, 6 g KH_2PO_4, 1 mL 5 mg mL^{-1} cholesterol, H_2O to 1 L. Sterilize by autoclaving), 10 mL 1 mol L^{-1} potassium citrate pH 6, 10 mL trace metals solution (1.86 g disodium EDTA, 0.69 g $FeSO_4·7H_2O$, 0.2 g $MnCl_2·4H_2O$, 0.29 g $ZnSO_4·7H_2O$, 0.025 g $CuSO_4·5H_2O$, H_2O to 1 L. Sterilize by autoclaving. Store in the dark), 3 mL 1 mol L^{-1} $CaCl_2$, 3 mL 1 mol L^{-1} $MgSO_4$. If for RNAi, add 1 mmol L^{-1} IPTG and 100 μg mL^{-1} carbenicillin. Add components using sterile technique.

Biochemistry

Protein purification, mass spec analysis and Co-IP analysis

Synchronized young adult stage worms grown on EV or *cco-1* RNAi were collected and washed with M9 buffer. After washing 3 times, the suspension was then dripped into liquid N_2, and the resulting balls were ground using mortar and pestle. Add 0.5 volumes of extraction buffer (100 mmol L^{-1} Tris-HCl, pH 7.4, 1 mol L^{-1} NaCl, 1% NP-40, 10 mmol L^{-1} DTT, EDTA-free protease inhibitor cocktail (Roche, Switzerland), 2 mmol L^{-1} β-glycerophosphate, 2 mmol L^{-1} sodium orthovanadate, 2 mmol L^{-1} sodium pyrophosphate, 10 mmol L^{-1} sodium fluoride, and 2 mmol L^{-1} PMSF), lysed at 4°C for 30 min. The homogenized worm tissue was diluted NaCl to 150 mmol L^{-1} by adding dilute buffer (50 mmol L^{-1} Tris-HCl, pH 7.4, 5 mmol L^{-1} DTT, EDTA-free protease inhibitor cocktail (Roche), 2 mmol L^{-1} β-glycerophosphate, 2 mmol L^{-1} sodium orthovanadate, 2 mmol L^{-1} sodium pyrophosphate, 10 mmol L^{-1} sodium fluoride, and 2 mmol L^{-1} PMSF), and the insoluble materials were then removed by centrifugation for 10 min at 15,800×*g* at 4°C.

For IP-MS, 10 mL of lysate was mixed with GFP-trap agarose (Chromotek, Wuhan, China) (100 μL) for 4 h and washed for five times with wash buffer (50 mmol L^{-1} Tris-HCl pH 7.4, 150 mmol L^{-1} NaCl, and protease inhibitors). Proteins were eluted using 1% SDS by boiling and then subjected to MS analysis.

For immunoprecipitation, 5 mL lysates were mixed with 50 μL GFP-trap Agarose (Chromotek) for 4 h. Immunoprecipitates were

https://doi.org/10.1007/s11427-025-2954-3

washed five times with wash buffer (50 mmol L^{-1} Tris-HCl, pH 7.4; 150 mmol L^{-1} NaCl). Before running the Western blot, 5× SDS loading buffer was added to each sample, mixed well, and boiled for 15 min and resolved by SDS-polyacrylamide gel electrophoresis.

For coimmunoprecipitation, 2 mL of lysate was mixed with GFP-trap agarose (Chromotek) (20 μL) for 4 h. Immuno-precipitate was washed for five times with wash buffer (50 mmol L^{-1} Tris-HCl pH 7.4, 150 mmol L^{-1} NaCl, and protease inhibitors). Samples were then subjected to Western blot analysis.

Phos-specific antibody preparation

Antigen synthesis, animal immunization and antibody purification were done by ABclonal Biotechnology Co., Ltd. (Wuhan, China). Phospho-peptide antigen sequence is C-SNG(T-p)PASQ, non-phospho-peptide antigen sequence is C-SNGTPASQ. All peptide-specific antibodies are captured during affinity purification with the phosphopeptide. This fraction contains antibodies that recognize the phosphopeptide as well as antibodies that detect non-phosphopeptides. To get rid of the last ones, we use a non-phosphopeptide depletion.

Western blot analysis

For large-scale experiments, age-synchronized worms were washed off the plate with M9 buffer and frozen in liquid nitrogen. For small-scale experiments, 100 to 150 worms were picked into 16 μL of M9 buffer and frozen in liquid nitrogen. Before running the Western blot, SDS loading buffer was added to each sample, mixed well, and boiled for 15 min and resolved by SDS-polyacrylamide gel electrophoresis (Bio-Rad, USA) before blotting to a NC membrane. Antibodies used in this study were listed in Table S6.

For phos-detection, the membrane was blocked with 5% BSA-TBST (0.5% Tween-20) for 1 h, and then was washed with TBST (0.2% Tween-20) for 10 min, repeat 3 times. Then the membrane was incubated with Phos-specific antibody E17547P diluted with 5%BSA-TBST (0.5% Tween-20) overnight at 4°C, and then was washed with TBST (0.2% Tween-20) for 10 min, repeat 3 times. Incubate the membrane with secondary antibody for 1 h at room temperature in TBST. Wash the membrane 3 times in TBST.

Dot blot analysis

1 μL of 100 ng peptides was dropped onto NC membrane. Incubate the NC membrane at 37°C for 30 min. Block the membrane with 5% milk in TBST (50 mmol L^{-1} Tris, 0.5 mol L^{-1} NaCl, 0.1% Tween-20, pH 7.4) for 1 h at room temperature. Pour off the block buffer, but keep membrane wet at all times for the remainder of the procedure. Incubate the membrane with primary antibody for 2 h at room temperature in 5% milk-TBST (0.1% Tween-20). Wash the membrane 3 times in TBST. Incubate the membrane with secondary antibody for 1 h at room temperature in TBST. Wash the membrane 3 times in TBST.

Construction and expression of recombinant proteins

To generate recombinant proteins GST-GSP-2, cDNA of *gsp-2* was subcloned into pGEX-4T-2 for GST-fused proteins. To generate recombinant proteins 6×His-Myc-DVE-1 and 6×His-Flag-HDA-1, cDNA of dve-1 and hda-1 were subcloned into pET28a(+) for poly-histidine-tagged (6×His) proteins. Transform the expression plasmid into *E. coli* BL21. Incubate bacteria at 37°C with shaking until A_{600} reaches 0.4–0.8. For most vector systems, induce with 1 mmol L^{-1} IPTG and express protein for 4 h at 37°C. The induced bacteria were collected and sonicated, then the supernatant was collected for purifying proteins following the manual. BeyoGoldTM GST-tag Purification Resin (Beyotime, Shanghai, China) was used to purify GST-fused proteins. Ni Sepharose 6 Fast Flow (GE Healthcare, USA) was used for purification of 6×His proteins.

Life-span analysis

Lifespan experiments were performed on NGM plates at 20°C as previously described (Dillin et al., 2002). To prevent progeny production, 200 μL of 10 mg mL^{-1} 5-fluoro-2′-deoxyuridine (FUdR) was added to seeded plates. Worms were synchronized by egg bleach and were grown on OP50 bacteria from hatch, and transferred to FUdR plates at day 1 stage. Worms were scored every second day. All lifespan data are available in Table S3. Prism 10 software was used for statistical analysis. Log-rank (Mantel-Cox) method was used to determine the significance difference.

OCR

OCR measurements were performed using Seahorse XFe-96 analyser (Agilent, USA). OCR was assessed on day 1 of adulthood. Worms were collected and washed for three times with M9 to get rid of the traces of bacteria. Ten worms were transferred to each well of Seahorse XF-96 cell culture microplates, containing 200 μL M9. OCR was measured 10 cycles (7 min/cycle) under basal conditions. Each measurement was repeated at least six times.

Brood size assay

Single worms were individually transferred to plates and moved to fresh dishes daily until egg-laying ceased. The number of eggs was recorded every day. The nematode brood size was determined based on the sum of total eggs laid by individual hermaphrodites.

Statistical analysis

All experiments were repeated at least two times with identical or similar results. Data represent biological replicates. Appropriate statistical tests were used for every figure. Data met the assumptions of the statistical tests described for each figure. Statistical parameters, including the exact value of n and descriptive statistics (mean±SEM) and statistical significance, are reported in the figures and the figure legends.

Data availability

All unique/stable resources generated in this study will be made available from the lead contact with a completed Material Transfer Agreement.

Compliance and ethics

The authors declare that they have no conflict of interest.

Acknowledgement

This work was supported by the National Key Research and Development Program of China (2022YFA1303000), the Strategic Priority Research Program of the Chinese Academy of Sciences (XDB39000000), the National Natural Science Foundation of China (32371214, 32225025, 92254305, 32321004, 32430025), the CAS Project for Young Scientists in Basic Research (YSBR-076), and the Youth Innovation Promotion Association CAS (2021094). Y. T. is supported by the New Cornerstone Science Foundation through the XPLORER PRIZE. Several *C. elegans* strains used in this work were provided by the Caenorhabditis Genetics Center (CGC), funded by the NIH P40OD010440. We thank Tian lab members for the insightful discussions and Y. Liu for helping with strain maintenance..

Supporting information

The supporting information is available online at https://doi.org/10.1007/s11427-025-2954-3. The supporting materials are published as submitted, without typesetting or editing. The responsibility for scientific accuracy and content remains entirely with the authors.

References

Ahier, A., Dai, C.Y., Tweedie, A., Bezawork-Geleta, A., Kirmes, I., and Zuryn, S. (2018). Affinity purification of cell-specific mitochondria from whole animals resolves patterns of genetic mosaicism. Nat Cell Biol 20, 352–360.

Arur, S., and Schedl, T. (2014). Generation and purification of highly specific antibodies for detecting post-translationally modified proteins *in vivo*. Nat Protoc 9, 375–395.

Basta, J., and Rauchman, M. (2015). The nucleosome remodeling and deacetylase complex in development and disease. Transl Res 165, 36–47.

Benedetti, C., Haynes, C.M., Yang, Y., Harding, H.P., and Ron, D. (2006). Ubiquitin-like protein 5 positively regulates chaperone gene expression in the mitochondrial unfolded protein response. Genetics 174, 229–239.

Bennett, C.F., Vander Wende, H., Simko, M., Klum, S., Barfield, S., Choi, H., Pineda, V. V., and Kaeberlein, M. (2014). Activation of the mitochondrial unfolded protein response does not predict longevity in *Caenorhabditis elegans*. Nat Commun 5, 3483.

Bornelöv, S., Reynolds, N., Xenophontos, M., Gharbi, S., Johnstone, E., Floyd, R., Ralser, M., Signolet, J., Loos, R., Dietmann, S., et al. (2018). The nucleosome remodeling and deacetylation complex modulates chromatin structure at sites of active transcription to fine-tune gene expression. Mol Cell 71, 56–72.e4.

Bottardi, S., Mavoungou, L., Pak, H., Daou, S., Bourgoin, V., Lakehal, Y.A., Affar, E.B., Milot, E., and Grimes, H.L. (2014). The IKAROS interaction with a complex including chromatin remodeling and transcription elongation activities is required for hematopoiesis. PLoS Genet 10, e1004827.

Bouazoune, K., and Brehm, A. (2005). dMi-2 chromatin binding and remodeling activities are regulated by dCK2 phosphorylation. J Biol Chem 280, 41912–41920.

Brenner, S. (1974). The genetics of *Caenorhabditis elegans*. Genetics 77, 71–94.

Cai, Y., Song, W., Li, J., Jing, Y., Liang, C., Zhang, L., Zhang, X., Zhang, W., Liu, B., An, Y., et al. (2022). The landscape of aging. Sci China Life Sci 65, 2354–2454.

Chen, M.J., Dixon, J.E., and Manning, G. (2017). Genomics and evolution of protein phosphatases. Sci Signal 10, eaag1796.

Chen, P.X., Zhang, L., Chen, D., and Tian, Y. (2024). Mitochondrial stress and aging: lessons from *C. elegans*. Semin Cell Dev Biol 154, 69–76.

Copeland, J.M., Cho, J., Lo Jr., T., Hur, J.H., Bahadorani, S., Arabyan, T., Rabie, J., Soh, J., and Walker, D.W. (2009). Extension of drosophila life span by RNAi of the mitochondrial respiratory chain. Curr Biol 19, 1591–1598.

De Vaux, V., Pfefferli, C., Passannante, M., Belhaj, K., von Essen, A., Sprecher, S.G., Müller, F., and Wicky, C. (2013). The *Caenorhabditis elegans* LET-418/Mi2 plays a conserved role in lifespan regulation. Aging Cell 12, 1012–1020.

Dillin, A., Hsu, A.L., Arantes-Oliveira, N., Lehrer-Graiwer, J., Hsin, H., Fraser, A.G., Kamath, R.S., Ahringer, J., and Kenyon, C. (2002). Rates of behavior and aging specified by mitochondrial function during development. Science 298, 2398–2401.

Fessler, E., Eckl, E.M., Schmitt, S., Mancilla, I.A., Meyer-Bender, M.F., Hanf, M., Philippou-Massier, J., Krebs, S., Zischka, H., and Jae, L.T. (2020). A pathway coordinated by DELE1 relays mitochondrial stress to the cytosol. Nature 579, 433–437.

Ganju, A., Chauhan, S.C., Hafeez, B.B., Doxtater, K., Tripathi, M.K., Zafar, N., Yallapu, M.M., Kumar, R., and Jaggi, M. (2018). Protein kinase D1 regulates subcellular localisation and metastatic function of metastasis-associated protein 1. Br J Cancer 118, 587–599.

Gao, Y., Zamisch, M., Vacchio, M., Chopp, L., Ciucci, T., Paine, E.L., Lyons, G.C., Nie, J., Xiao, Q., Zvezdova, E., et al. (2022). NuRD complex recruitment to Thpok mediates CD4$^+$ T cell lineage differentiation. Sci Immunol 7, eabn5917.

Genoux, D., Haditsch, U., Knobloch, M., Michalon, A., Storm, D., and Mansuy, I.M. (2002). Protein phosphatase 1 is a molecular constraint on learning and memory. Nature 418, 970–975.

Green, C.L., Lamming, D.W., and Fontana, L. (2022). Molecular mechanisms of dietary restriction promoting health and longevity. Nat Rev Mol Cell Biol 23, 56–73.

Guo, X., Aviles, G., Liu, Y., Tian, R., Unger, B.A., Lin, Y.H.T., Wiita, A.P., Xu, K., Correia, M.A., and Kampmann, M. (2020). Mitochondrial stress is relayed to the cytosol by an OMA1-DELE1-HRI pathway. Nature 579, 427–432.

Haynes, C.M., Petrova, K., Benedetti, C., Yang, Y., and Ron, D. (2007). ClpP mediates activation of a mitochondrial unfolded protein response in *C. elegans*. Dev Cell 13, 467–480.

Haynes, C.M., Yang, Y., Blais, S.P., Neubert, T.A., and Ron, D. (2010). The matrix peptide exporter HAF-1 signals a mitochondrial UPR by activating the transcription factor ZC376.7 in *C. elegans*. Mol Cell 37, 529–540.

Hornbeck, P.V., Zhang, B., Murray, B., Kornhauser, J.M., Latham, V., and Skrzypek, E. (2015). PhosphoSitePlus, 2014: mutations, PTMs and recalibrations. Nucleic Acids Res 43, D512–D520.

Kloet, S.L., Karemaker, I.D., van Voorthuijsen, L., Lindeboom, R.G.H., Baltissen, M.P., Edupuganti, R.R., Poramba-Liyanage, D.W., Jansen, P.W.T.C., and Vermeulen, M. (2018). NuRD-interacting protein ZFP296 regulates genome-wide NuRD localization and differentiation of mouse embryonic stem cells. Nat Commun 9, 4588.

Lai, A.Y., and Wade, P.A. (2011). Cancer biology and NuRD: a multifaceted chromatin remodelling complex. Nat Rev Cancer 11, 588–596.

Lee, S.S., Lee, R.Y.N., Fraser, A.G., Kamath, R.S., Ahringer, J., and Ruvkun, G. (2003). A systematic RNAi screen identifies a critical role for mitochondria in *C. elegans* longevity. Nat Genet 33, 40–48.

Li, J., Cui, J., Li, X., Zhu, D., Chen, Z., Huang, X., Wang, Y., Wu, Q., and Tian, Y. (2025). TMBIM-2 orchestrates systemic mitochondrial stress response via facilitating Ca^{2+} oscillations. J Cell Biol 224, e202408050.

Li, J., Cui, J., and Tian, Y. (2022a). Neuron-periphery mitochondrial stress communication in aging and diseases. Life Med 1, 168–178.

Li, T.Y., Sleiman, M.B., Li, H., Gao, A.W., Mottis, A., Bachmann, A.M., Alam, G.E., Li, X., Goeminne, L.J.E., Schoonjans, K., et al. (2021). The transcriptional coactivator CBP/p300 is an evolutionarily conserved node that promotes longevity in response to mitochondrial stress. Nat Aging 1, 165–178.

Li, X., Li, J., Zhu, D., Zhang, N., Hao, X., Zhang, W., Zhang, Q., Liu, Y., Wu, X., and Tian, Y. (2022b). Protein disulfide isomerase PDI-6 regulates Wnt secretion to coordinate inter-tissue UPR^{mt} activation and lifespan extension in *C. elegans*. Cell Rep 39, 110931.

Lima, T., Li, T.Y., Mottis, A., and Auwerx, J. (2022). Pleiotropic effects of mitochondria in aging. Nat Aging 2, 199–213.

Liu, X., Jiang, N., Hughes, B., Bigras, E., Shoubridge, E., and Hekimi, S. (2005). Evolutionary conservation of the *clk-1*-dependent mechanism of longevity: loss of *mclk1* increases cellular fitness and lifespan in mice. Genes Dev 19, 2424–2434.

Liu, Y., Zhou, J., Zhang, N., Wu, X., Zhang, Q., Zhang, W., Li, X., and Tian, Y. (2022). Two sensory neurons coordinate the systemic mitochondrial stress response via GPCR signaling in *C. elegans*. Dev Cell 57, 2469–2482.e5.

López-Otín, C., Blasco, M.A., Partridge, L., Serrano, M., and Kroemer, G. (2013). The hallmarks of aging. Cell 153, 1194–1217.

López-Otín, C., Blasco, M.A., Partridge, L., Serrano, M., and Kroemer, G. (2023). Hallmarks of aging: an expanding universe. Cell 186, 243–278.

Merkwirth, C., Jovaisaite, V., Durieux, J., Matilainen, O., Jordan, S.D., Quiros, P.M., Steffen, K.K., Williams, E.G., Mouchiroud, L., Tronnes, S.U., et al. (2016). Two conserved histone demethylases regulate mitochondrial stress-induced longevity. Cell 165, 1209–1223.

Mottis, A., Herzig, S., and Auwerx, J. (2019). Mitocellular communication: shaping health and disease. Science 366, 827–832.

Nargund, A.M., Pellegrino, M.W., Fiorese, C.J., Baker, B.M., and Haynes, C.M. (2012). Mitochondrial import efficiency of ATFS-1 regulates mitochondrial UPR activation. Science 337, 587–590.

Pegoraro, G., Kubben, N., Wickert, U., Göhler, H., Hoffmann, K., and Misteli, T. (2009). Ageing-related chromatin defects through loss of the NURD complex. Nat Cell Biol 11, 1261–1267.

Picard, M., and Shirihai, O.S. (2022). Mitochondrial signal transduction. Cell Metab 34, 1620–1653.

Polo, S.E., Kaidi, A., Baskcomb, L., Galanty, Y., and Jackson, S.P. (2010). Regulation of DNA-damage responses and cell-cycle progression by the chromatin remodelling factor CHD4. EMBO J 29, 3130–3139.

Rea, S.L., Ventura, N., Johnson, T.E., and Kirkwood, T.B.L. (2007). Relationship between mitochondrial electron transport chain dysfunction, development, and life extension in *Caenorhabditis elegans*. PLoS Biol 5, e259.

Reid, X.J., Low, J.K.K., and Mackay, J.P. (2023). A NuRD for all seasons. Trends Biochem Sci 48, 11–25.

Roh, J., Rhee, J., Chaudhari, V., and Rosenzweig, A. (2016). The role of exercise in cardiac aging: from physiology to molecular mechanisms. Circ Res 118, 279–295.

Shao, L.W., Peng, Q., Dong, M., Gao, K., Li, Y., Li, Y., Li, C.Y., and Liu, Y. (2020). Histone deacetylase HDA-1 modulates mitochondrial stress response and longevity. Nat Commun 11, 4639.

Shen, K., Pender, C.L., Bar-Ziv, R., Zhang, H., Wickham, K., Willey, E., Durieux, J.,

Ahmad, Q., and Dillin, A. (2022). Mitochondria as cellular and organismal signaling hubs. Annu Rev Cell Dev Biol 38, 179–218.
Shpilka, T., and Haynes, C.M. (2018). The mitochondrial UPR: mechanisms, physiological functions and implications in ageing. Nat Rev Mol Cell Biol 19, 109–120.
Sujkowski, A., Hong, L., Wessells, R.J., and Todi, S.V. (2022). The protective role of exercise against age-related neurodegeneration. Ageing Res Rev 74, 101543.
Sun, J.M., Chen, H.Y., and Davie, J.R. (2007). Differential distribution of unmodified and phosphorylated histone deacetylase 2 in chromatin. J Biol Chem 282, 33227–33236.
Sutandy, F.X.R., Gößner, I., Tascher, G., and Münch, C. (2023). A cytosolic surveillance mechanism activates the mitochondrial UPR. Nature 618, 849–854.
Tan, J.X., and Finkel, T. (2020). Mitochondria as intracellular signaling platforms in health and disease. J Cell Biol 219, e202002179.
Templeman, N.M., and Murphy, C.T. (2018). Regulation of reproduction and longevity by nutrient-sensing pathways. J Cell Biol 217, 93–106.
Tian, Y., Garcia, G., Bian, Q., Steffen, K.K., Joe, L., Wolff, S., Meyer, B.J., and Dillin, A. (2016). Mitochondrial stress induces chromatin reorganization to promote longevity and UPR^{mt}. Cell 165, 1197–1208.
Wang, B., Li, C., Ming, J., Wu, L., Fang, S., Huang, Y., Lin, L., Liu, H., Kuang, J., Zhao, C., et al. (2023). The NuRD complex cooperates with SALL4 to orchestrate reprogramming. Nat Commun 14, 2846.
Wang, Z., Zhang, Q., Jiang, Y., Zhou, J., and Tian, Y. (2024). ASI-RIM neuronal axis regulates systemic mitochondrial stress response via TGF-β signaling cascade. Nat Commun 15, 8997.
Wu, Z., Qu, J., Zhang, W., and Liu, G.H. (2024). Stress, epigenetics, and aging: unraveling the intricate crosstalk. Mol Cell 84, 34–54.
Xing, J., Chen, K., Gao, S., Pousse, M., Ying, Y., Wang, B., Chen, L., Wang, C., Wang, L., Hu, W., et al. (2023). Protein phosphatase 2A activators reverse age-related behavioral changes by targeting neural cell senescence. Aging Cell 22, e13780.
Yu, X., Zhao, P., Luo, Q., Wu, X., Wang, Y., Nan, Y., Liu, S., Gao, W., Li, B., Liu, Z., et al. (2024). RUNX1-IT1 acts as a scaffold of STAT1 and NuRD complex to promote ROS-mediated NF-κB activation and ovarian cancer progression. Oncogene 43, 420–433.
Zhang, Q., Wu, X., Chen, P., Liu, L., Xin, N., Tian, Y., and Dillin, A. (2018). The mitochondrial unfolded protein response is mediated cell-non-autonomously by retromer-dependent Wnt signaling. Cell 174, 870–883.e17.
Zhao, Z., Sentürk, N., Song, C., and Grummt, I. (2018). lncRNA PAPAS tethered to the rDNA enhancer recruits hypophosphorylated CHD4/NuRD to repress rRNA synthesis at elevated temperatures. Genes Dev 32, 836–848.
Zhu, D., Li, X., and Tian, Y. (2022). Mitochondrial-to-nuclear communication in aging: an epigenetic perspective. Trends Biochem Sci 47, 645–659.
Zhu, D., Wu, X., Zhou, J., Li, X., Huang, X., Li, J., Wu, J., Bian, Q., Wang, Y., and Tian, Y. (2020). NuRD mediates mitochondrial stress-induced longevity via chromatin remodeling in response to acetyl-CoA level. Sci Adv 6, eabb2529.
Zimmerman, S.M., and Kim, S.K. (2014). The GATA transcription factor/MTA-1 homolog *egr-1* promotes longevity and stress resistance in *Caenorhabditis elegans*. Aging Cell 13, 329–339.